Measurement of the binding energy of ultracold $^{87}Rb^{133}Cs$ molecules using an offset-free optical frequency comb

Peter K. Molony,[1] Avinash Kumar,[1] Philip D. Gregory,[1] Russell Kliese,[2] Thomas Puppe,[2] C. Ruth Le Sueur,[3] Jesus Aldegunde,[4] Jeremy M. Hutson,[3] and Simon L. Cornish[1,*]

[1]*Joint Quantum Centre (JQC) Durham-Newcastle, Department of Physics, Durham University, South Road, Durham DH1 3LE, United Kingdom*

[2]*TOPTICA Photonics AG, Lochhamer Schlag 19, Gräfelfing 82166, Germany*

[3]*Joint Quantum Centre (JQC) Durham-Newcastle, Department of Chemistry, Durham University, South Road, Durham DH1 3LE, United Kingdom*

[4]*Departamento de Quimica Fisica, Universidad de Salamanca, 37008 Salamanca, Spain*

(Received 27 May 2016; published 15 August 2016)

We report the binding energy of $^{87}Rb^{133}Cs$ molecules in their rovibrational ground state measured using an offset-free optical frequency comb based on difference frequency generation technology. We create molecules in the absolute ground state using stimulated Raman adiabatic passage (STIRAP) with a transfer efficiency of 88%. By measuring the absolute frequencies of our STIRAP lasers, we find the energy-level difference from an initial weakly bound Feshbach state to the rovibrational ground state with a resolution of ∼5 kHz over an energy-level difference of more than 114 THz; this lets us discern the hyperfine splitting of the ground state. Combined with theoretical models of the Feshbach-state binding energies and ground-state hyperfine structure, we determine a zero-field binding energy of $h \times 114\,268\,135.24(4)(3)$ MHz. To our knowledge, this is the most accurate determination to date of the dissociation energy of a molecule.

DOI: 10.1103/PhysRevA.94.022507

I. INTRODUCTION

Quantum gases of polar molecules have received great attention in recent years. Their long-range interactions and rich internal structure hold enormous potential in the fields of quantum many-body simulations [1,2], quantum computation [3], ultracold chemistry [4,5], and precision measurement of fundamental constants [6–10]. It is only recently, however, that a few such molecules (KRb, RbCs, NaK, NaRb) have been successfully trapped at ultracold temperatures in their rovibrational ground state [11–15], making them available for experimental study. These experiments all share a common technique for the production of molecules, in which atoms are first associated to form weakly bound molecules by tuning a magnetic field across a Feshbach resonance, and the molecules are then transferred optically to the ground state using stimulated Raman adiabatic passage (STIRAP) [16,17].

Accurate characterization of the internal structure of these molecules has been challenging both theoretically and experimentally. The most precise measurement so far of the binding energy of these molecules is for KRb [11], where a frequency comb was used to measure the difference in laser frequency for the STIRAP transfer to a precision of ±1 MHz at a nonzero magnetic field. In $^{87}Rb^{133}Cs$, the measurement precision has so far been approximately 20 MHz, limited by the precision of wavemeters [13,18].

It has been proposed [8] that precision spectroscopy of certain molecules could be used to make sensitive measurements of the variation of fundamental constants, particularly the electron-proton mass ratio [9,10,19] and the fine-structure constant [9,20]. Previous studies have focused on microwave transitions [20,21] and high-lying vibrational states [22–24]. Using an optical frequency comb reference, the high precision afforded by measurements on ultracold molecules can in principle be extended to arbitrary vibrational states. The demonstration that molecular transitions in the optical domain can be measured with fractional uncertainties below 10^{-10} represents an important step toward measuring the variation of fundamental constants in ultracold molecules.

In this article, we present the most precise measurement of the binding energy D_0, or dissociation energy, of the lowest rovibrational level of the $^{87}Rb^{133}Cs$ $X^1\Sigma^+$ electronic ground state. We begin with a brief overview of the method we use to create samples of ultracold ground-state $^{87}Rb^{133}Cs$ molecules. We explain the working and stability of our frequency comb based on difference frequency generation and how we use it to measure the 114-THz frequency difference between the STIRAP lasers. From this frequency difference we use theoretical models of the molecular structure to calculate the binding energy of the $^{87}Rb^{133}Cs$ molecule at zero magnetic field.

II. CREATING GROUND-STATE MOLECULES

Details of our experimental setup may be found in our previous publications [25–29]. Briefly, from a two-species magneto-optical trap we load both species into a magnetic trap [25]. We use forced radio-frequency (RF) evaporation [26], followed by plain evaporation in a levitated optical trap ($\lambda = 1550$ nm) [27], to create a high-phase-space-density mixture of $\sim 3.0 \times 10^5$ atoms of each species at a temperature of ∼300 nK [28]. Molecules are produced from this atomic mixture by sweeping the magnetic field across an interspecies Feshbach resonance at 197.10(3) G at a rate of 250 G s^{-1} [29]. After magnetoassociation, molecules populate the near-threshold $|-1(1,3)s(1,3)\rangle$ spin-stretched bound state of the

*s.l.cornish@durham.ac.uk

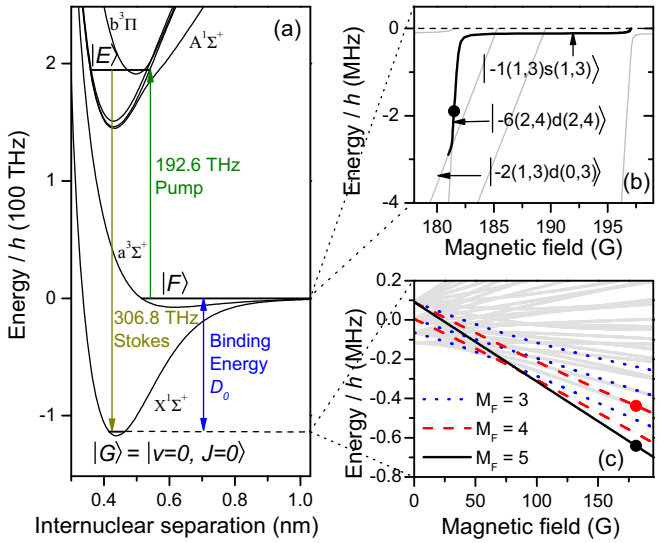

FIG. 1. ^{87}Rb^{133}Cs molecular states relevant to our experiment. (a) Position of the energy levels we use for STIRAP within the molecular potentials. The initial Feshbach state, intermediate excited state, and ground state are labeled $|F\rangle$, $|E\rangle$, and $|G\rangle$ respectively. (b) Molecular states close to dissociation. The dotted line is the Rb $|f = 1, m_f = 1\rangle$ + Cs $|3,3\rangle$ threshold. The black line shows the path followed by the molecules directly after magnetoassociation at the Feshbach resonance at 197.10(3) G. (c) Zeeman splitting of the ground state into 32 energy levels from total molecular nuclear spin $I'' = 2$, 3, 4, and 5. Transitions to the highlighted states are allowed by selection rules. Dots indicate the states we address with our laser system.

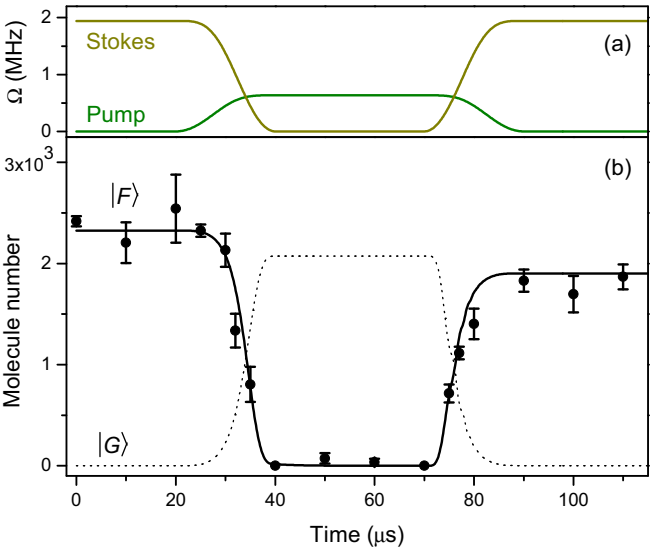

FIG. 2. STIRAP transfer to the molecular ground state and back. (a) Rabi frequency profile used for STIRAP transfer. (b) Experimentally measured population of the Feshbach state $|F\rangle$ throughout the transfer process. The sequence keeps the molecules in the ground state for 30 μs before transferring them back to the initial state for dissociation and absorption imaging. We show a numerical model of the Feshbach- and ground-state populations based on the Lindblad master equation for an open three-level system, including the effects of the laser linewidth. The one-way transfer efficiency is 88%. The optical trap is switched off throughout the sequence.

potential $a^3\Sigma^+$ as shown in Fig. 1(b). Here, states are labeled $|n(f_{\rm Rb}, f_{\rm Cs})L(m_{f_{\rm Rb}}, m_{f_{\rm Cs}})\rangle$, where n is the vibrational quantum number counted downward from the dissociation threshold for the particular hyperfine $(f_{\rm Rb}, f_{\rm Cs})$ manifold, and L is the standard letter designation for the molecular rotational angular momentum quantum number [30]. The coupling between the $|-6(2,4)d(2,4)\rangle$ state and the excited state is strong enough to allow STIRAP transfer to the ground state. However, this state is low field seeking and cannot be magnetically levitated in our system. Thus we cannot selectively remove the atoms while trapping the molecules in the $|-6(2,4)d(2,4)\rangle$ state. We therefore transfer our molecules to the high-field-seeking, weakly bound $|-2(1,3)d(0,3)\rangle$ state by reducing the magnetic field to ~180.5 G, at which point the atoms and molecules are separated using the Stern-Gerlach effect (at a field gradient of 44 G cm^{-1}, which levitates the molecules), taking advantage of their different magnetic moments when the molecules are in this state. We then reduce the magnetic field gradient and ramp up the dipole trap to create a pure optical trap. Finally, the magnetic field is ramped to ~181.5 G. This results in ~2500 molecules in the $|-6(2,4)d(2,4)\rangle$ state at a temperature of 1.5 μK.

The weakly bound molecules are transferred to the rovibrational ground state optically using STIRAP. We couple both the initial near-dissociation state and the ground state to a common excited state. This excited state is chosen to be the $|\Omega' = 1, v' = 29, J' = 1\rangle$ state, from the coupled $A^1\Sigma^+ + b^3\Pi$ potential, because it has strong couplings to both the Feshbach and the ground states [12]. The pump and Stokes lasers are shown schematically in Fig. 1(a) and have frequencies of 192.6 THz (1557 nm) and 306.8 THz (977 nm), respectively. For coherent transfer, we narrow the linewidth of both the pump and the Stokes lasers to <1 kHz by frequency stabilization to a fixed-length high-finesse optical cavity constructed from ultralow-expansion glass by ATFilms. Continuous tuning is given by a pair of fiber-coupled electro-optic modulators. Further details of the laser system can be found in [31].

We transfer the molecules to the ground state and back as shown in Fig. 2. This figure shows a model of the Lindblad master equation for an open three-level system as described in our previous work [13]. We use our measured peak Rabi frequencies of $2\pi \times 0.6$ and $2\pi \times 1.9$ MHz for the pump and Stokes transitions, respectively, and our measured excited-state linewidth of $2\pi \times 35(3)$ kHz. We extend the model used in Ref. [13] to include a Monte Carlo simulation of the laser noise [32]. The model has no free parameters. Further details of this model are presented in a separate publication [33]. As the dipole trapping wavelength is close to the pump transition, it induces an ac Stark shift of ~0.5 MHz. This shift varies across the cloud because of the finite size of the molecular cloud and trapping beams, reducing the efficiency of the transfer. To avoid this we switch our dipole trap off for 200 μs during the STIRAP transfer to and from the ground state. This improves our one-way transfer efficiency from 50% [13] to 88%, creating a sample of over 2000 molecules in the rovibrational ground state.

III. LASER FREQUENCY MEASUREMENT

We determine the binding energy with precision measurements of the pump and Stokes transition frequencies using a GPS-referenced frequency comb. Our frequency comb is the first of its kind, based on difference frequency generation technology developed by TOPTICA Photonics AG [34]. In this comb, the amplified output of an Er:fiber oscillator is compressed using a silicon prism compressor and then spectrally broadened using a highly nonlinear photonic crystal fiber to make a supercontinuum spanning more than an optical octave. The comb teeth in the spectrum are given by $f = Nf_{\mathrm{rep}} + f_{\mathrm{CEO}}$. Two extreme parts of this supercontinuum are spatially and temporally overlapped in a nonlinear difference frequency generation crystal. This cancels the carrier-envelope offset frequency (f_{CEO}) to produce an offset-free frequency comb spectrum at 1550 nm with a bandwidth of ~100 nm. Each comb tooth N then has a frequency $f = Nf_{\mathrm{rep}}$. This output is then extended to different wavelength ranges by nonlinear frequency shifting and frequency doubling. This method of canceling f_{CEO} has the advantage of requiring no servo-loop feedback system, compared to the conventional $f - 2f$ approach where the high-frequency noise components of f_{CEO} cannot be canceled [35]. The characterization of the phase noise of different comb teeth confirms the elastic tape model [36] with a fixed point at zero frequency [37].

The frequency comb is seeded by a mode-locked Er:fiber laser with an 80-MHz repetition rate, whose 10th harmonic is locked to an 800-MHz ultralow-noise oven-controlled RF oscillator, which in turn is locked to a 10-MHz GPS reference [38]. We have measured the absolute stability of the comb locked to the GPS reference by recording a beat note between a comb tooth and a laser stabilized to the Rb $5S_{1/2}(f = 2) \rightarrow 5P_{3/2}(f' = 3)$ line. Figure 3(a) shows the Allan deviation (AD) of the beat signal, compared to the AD of the GPS-referenced oscillator to which the comb is locked. The AD of the beat follows a trend similar to that of the reference signal but deviates at longer time scales. This deviation is due to the drift in the lock-signal offset of the laser locked to the Rb spectroscopy line and is commonly observed over such time scales. These results show that measuring uncertainties down to 10^{-11} is practical with our comb system.

To quantify the lock noise of the comb, we measure the AD of a beat signal between two combs locked to a common RF reference. We observe an overall AD lower than the reference signal with no similarity to the AD of the reference signal [Fig. 3(b)]. This indicates that the noise on the repetition rate lock is much smaller than the noise on the GPS reference, and the fractional uncertainty in the repetition rate exactly follows that of the GPS reference. Therefore we can consider the AD of the GPS signal at time scales greater than our experimental cycle to calculate the resulting deviation in the repetition rate.

The frequency difference between the two STIRAP lasers is measured with comb teeth separated by $\delta N = (306.8 - 192.6)\ \mathrm{THz}/80\ \mathrm{MHz} \sim 10^6$, so the uncertainty in the GPS clock frequency must be less than 10 mHz if we are to maintain an uncertainty in our measured laser frequency of less than 10 kHz. The AD over time scales shorter than the experimental cycle will add to the statistical error of the molecular round-trip signal. However, the AD over longer time scales will lead to a systematic offset in our measurements. From the specifications of the GPS reference we calculate that, over the course of one measurement, the AD leads to a systematic uncertainty of ±23 Hz in the frequency difference between the two lasers. This is negligible compared to the other sources of uncertainty described later.

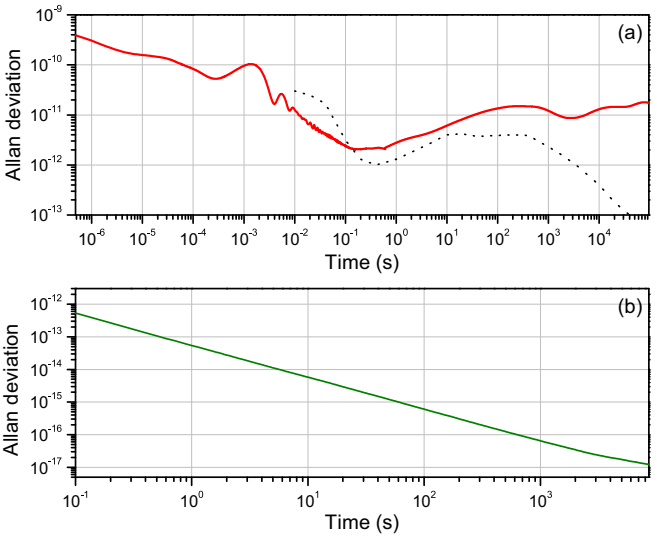

FIG. 3. Measurements of the stability of the frequency comb. (a) Allan deviation (AD) of a beat between the frequency comb and a laser stabilized to the Rb $5S_{1/2}(f = 2) \rightarrow 5P_{3/2}(f' = 3)$ transition (solid red line) and AD of the GPS-referenced 10-MHz oscillator (black dots) to which the comb is locked. (b) AD of the beat signal between two identical difference frequency generation combs locked to a common reference. The beat was recorded at a wavelength of 1556 nm via a transfer oscillator [37].

The absolute frequency of the lasers is measured by beating light from each of the STIRAP lasers with the nearest tooth of the optical frequency comb. A schematic of the optical setup used to measure the beat note and the comb tooth number is shown in Fig. 4. The beat note is recorded on a spectrum analyzer [39], which is referenced to the same 10-MHz GPS clock as the comb. The frequency of the beat note is averaged and recorded over each 3-s interval. We identify the nearest comb tooth (N) using a wavemeter with an absolute accuracy of 30 MHz [40], which we calibrate with lasers locked to well-known spectral lines in Rb, Cs, and Sr.

The light reaching the molecules is offset from that sent to the frequency comb by a pair of acousto-optic modulators (AOMs), at +80 MHz and −80 MHz for the pump and Stokes lasers, respectively. These provide the analog intensity ramps for STIRAP and are driven by fixed-frequency driver/amplifiers [41]. We measure the accuracy of the absolute frequency of these drivers with a spectrum analyzer [42] and find a constant offset of −705.0(3) Hz from the nominal 80 MHz. The statistical uncertainty in this offset is negligible.

IV. ENERGY DIFFERENCE MEASUREMENT

Maximum STIRAP transfer efficiency is achieved when the laser frequencies meet the two-photon resonance condition, while any common detuning of both lasers has relatively little

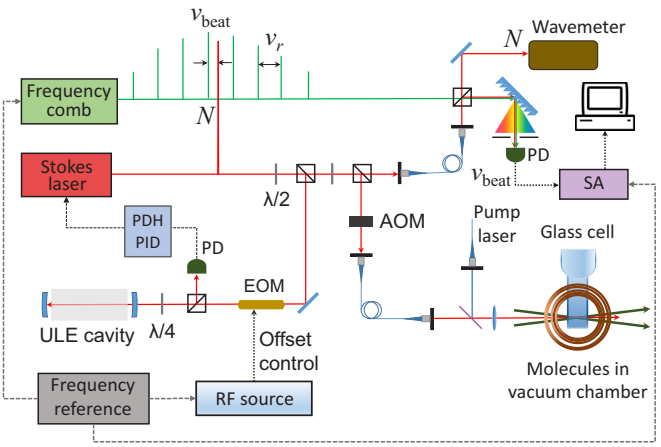

FIG. 4. Schematic of the experiment to carry out spectroscopy while recording the beat note (ν_{beat}) of the STIRAP lasers with the optical frequency comb. The beat signal between each STIRAP laser and the nearest comb line (N) is detected on a photodiode which is connected to a spectrum analyzer (SA). Both STIRAP lasers are frequency stabilized to a common ultralow-expansion cavity using the Pound-Drever-Hall method [43]. Continuous tuning of each laser is provided by varying the RF driving frequency of a broadband fiber-coupled electro-optic modulator (EOM). The light reaching the molecules is offset by 80 MHz from that sent to the frequency comb by an acousto-optic modulator (AOM) which modulates the intensity of the light. Further details of the frequency stabilization and tuning of the STIRAP lasers are given by Gregory *et al.* [31]. The frequency comb, spectrum analyzers, and EOM driver are all referenced to the same 10-MHz GPS disciplined oscillator. The figure shows the setup for the Stokes laser; the setup for the pump laser is identical.

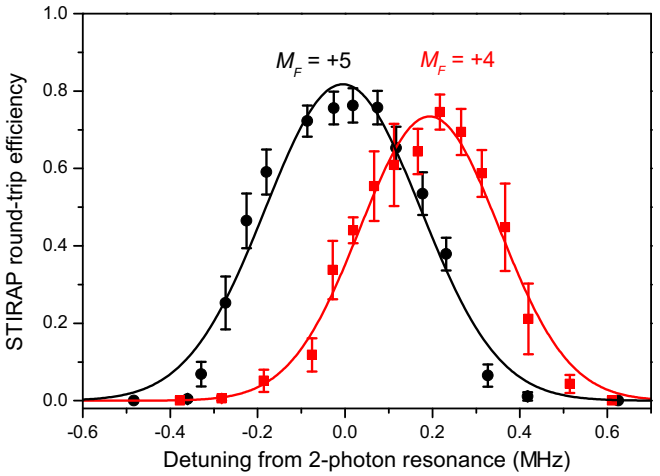

FIG. 5. STIRAP transfer to different hyperfine sublevels. The STIRAP round-trip transfer efficiency changes with the frequency difference of the pump and Stokes lasers for horizontal (black circles) and vertical (red squares) Stokes polarizations at a magnetic field of ∼181.5 G. Black circles show the transfer to the $M_F = +5$ state, while red squares show the $M_F = +4$ state. Gaussian fits give a separation between the states of 0.194(10) MHz.

effect on the efficiency [17,31]. By scanning their frequency difference and observing where we get maximum transfer efficiency, we determine the energy difference between the initial state $|F\rangle$ and the final state $|G\rangle$.

To measure the energy difference, we fix the frequency of the pump laser on resonance with the Feshbach and intermediate states. We then vary the frequency of the Stokes laser and measure the efficiency of the STIRAP transfer. The beat notes of both lasers with the optical frequency comb are measured throughout. For each data point we subtract the pump and Stokes absolute frequencies measured with the comb, and add the shifts from the AOMs, to get an absolute frequency difference. This gives us a peak as a function of the Stokes frequency which we fit to determine the energy difference between the initial and the final states, as shown in Fig. 5. The optimal Stokes frequency is determined over ∼4 h.

The precision with which we can locate the two-photon resonance is limited by the shot-to-shot noise in the number of molecules which we produce. This noise results in the vertical error bars shown in Fig. 5. The uncertainties in the detuning (horizontal error bars) are too small to be seen. A Gaussian fit gives an uncertainty in the center of the spectroscopic feature of around ±8 kHz. The magnetic field is measured before and after each complete measurement using the microwave transition frequency between the $|f = 3, m_f = +3\rangle$ and the $|4, +4\rangle$ states in atomic Cs.

We found the same frequency difference between the pump and the Stokes transition, within our experimental uncertainty, when using $|\Omega' = 0, v' = 35, J' = 1\rangle$ as an alternative intermediate state. This measurement was carried out using two-photon spectroscopy (where both the pump and the Stokes light are pulsed on simultaneously), as the coupling strengths are not high enough for efficient STIRAP transfer. The experimental procedure for two-photon spectroscopy of the ground state has been discussed previously by Molony *et al.* [13] and Gregory *et al.* [31]. This method, and the different transition strengths and linewidths, results in a much wider spectroscopic signal, leading to uncertainties two orders of magnitude larger in the two-photon resonance.

V. BINDING ENERGY CALCULATION

We now combine the measured energy difference and magnetic field with theoretical models to determine the energy difference between the degeneracy-weighted centers of the atomic and molecular hyperfine manifolds. We must correct for several shifts which are included in our measurement: the atomic hyperfine splittings, the Zeeman shifts of the $|1,1\rangle$ and $|3,3\rangle$ atomic states, the binding energy of the Feshbach molecule relative to these atomic states, and the molecular ground-state hyperfine splitting and Zeeman shift. The effects of all of these shifts are summarized in Table I. We discuss each of these below.

The Cs ground-state hyperfine splitting at zero field comes directly from the definition of the second, while the Rb splitting has been measured to <100 μHz [44]. These are weighted by the degeneracies of the atomic hyperfine states to give the distance to the $5^2S_{1/2} + 6^2S_{1/2}$ center. The atomic Zeeman splittings are calculated from the standard atomic Hamiltonian. The electron spin, electron orbital, and nuclear g factors are the

TABLE I. All the corrections, and their respective experimental errors, which must be added to each measurement of the energy difference $\nu_{\text{Stokes}} - \nu_{\text{pump}}$ to give the energy difference between the degeneracy-weighted hyperfine centroids of the free atoms and the RbCs rovibrational ground state, i.e., the binding energy. The uncertainty in the Zeeman shift is from the uncertainty in the measured magnetic field. Additional systematic uncertainties apply as explained in the text. Values listed are from the second measurement in Fig. 7 at a magnetic field 181.538(6) G driving a transition to the $M_F = 5$ hyperfine ground state. In Sec. VI we take an average of five such measurements. All values are in MHz.

Source	Correction (MHz)	Error (MHz)
$\nu_{\text{Stokes}} - \nu_{\text{pump}}$	114 258 363.067	0.006
Feshbach binding energy	1.84	0.04
Zeeman		
Rb	194.084	
Cs	134.353	
RbCs	−0.734	
Total		0.013
Hyperfine		
Cs	$\frac{9}{16} \times 9\,192.631\,770$	$\equiv 0$
Rb	$\frac{5}{8} \times 6\,834.682\,611$	$<10^{-10}$
RbCs ($I = 5$)	0.091	
Binding energy	114 268 135.23	0.04

values compiled by Steck [45]. We assume that the theoretical errors in these models are negligible.

We estimate the binding energy of the Feshbach state with respect to the $|1,1\rangle + |3,3\rangle$ threshold by combining the measurements and the coupled-channel model from Ref. [30], as shown in Fig. 6. There are nine experimental points for the $|-6(2,4)d(2,4)\rangle$ state between 181.4 and 181.9 G, and the coupled-channel model systematically underestimates the

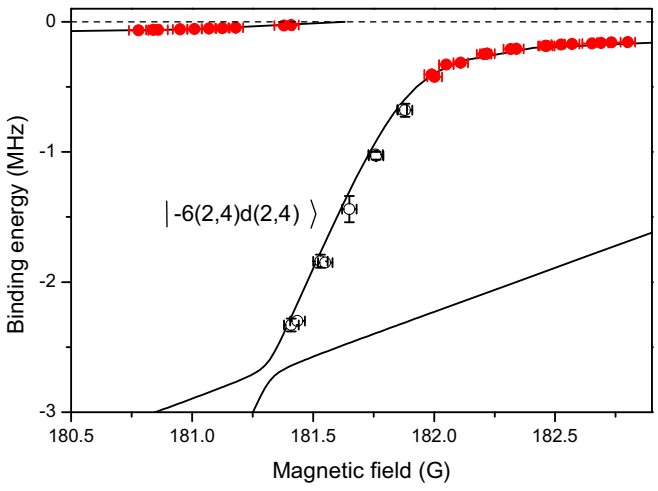

FIG. 6. Calculated positions of the highest-lying bound states for ^{87}Rb^{133}Cs (solid black lines) together with positions measured by free-bound magnetic-field modulation spectroscopy. Measurements included in the analysis of the required shifts of the binding energy (see text) are represented by open black circles; other data points in the set, by filled red circles. There are nine points included in the fit; some of them nearly overlap. Data taken from Takekoshi *et al.* [30].

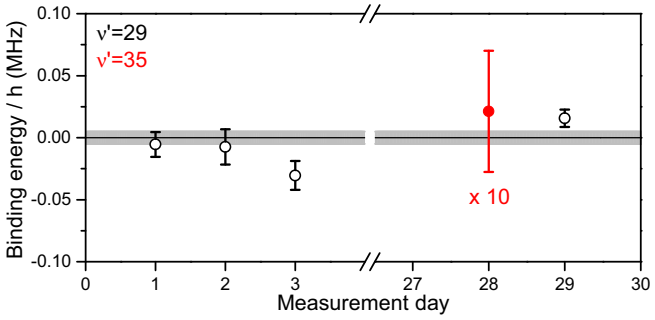

FIG. 7. Binding energy of the ^{87}Rb^{133}Cs molecule measured on different days. Statistical error bars are shown; additional systematic uncertainties apply as explained in the text. The vertical scale is offset by the mean value of 114 268 135.237 MHz. The gray-shaded region represents the 5-kHz experimental error on the mean. Open black (filled red) data points show the binding energy calculated from two-photon spectroscopy via $|\Omega' = 1, v' = 29, J' = 1\rangle$ ($|\Omega' = 0, v' = 35, J' = 1\rangle$) as the intermediate state. The $|\Omega' = 0, v' = 35, J' = 1\rangle$ measurement and error bar have been divided by 10 for clarity. The larger experimental errors in two-photon spectroscopy via the $|\Omega' = 0, v' = 35, J' = 1\rangle$ state are due to the poor signal-to-noise ratio of the molecular spectroscopy signal.

binding energies by 0.09 MHz. We correct for this deviation by fitting a global offset to the model in Fig. 6. This fitting has an experimental uncertainty of 0.04 MHz, which is shown in Table I but is not included in the statistical errors in Fig. 7 and Table II.

The $J = 0$ rovibrational ground state has four hyperfine levels with nuclear spins $I = 2$, 3, 4, and 5. In the presence of a magnetic field, these are split into 32 hyperfine and Zeeman states originating from the nuclear spin coupling to the magnetic field. These energy levels were calculated using the molecular Hamiltonian and parameters in Ref. [46] and are plotted in Fig. 1(c). We subtract both the hyperfine and the Zeeman shifts to give the binding energy of the ground-state hyperfine centroid, i.e., the origin of Fig. 1(c).

There are also theoretical uncertainties associated with the model of the ground-state hyperfine structure. The hyperfine splitting of the $I = 2$, 3, 4, and 5 states is determined almost entirely by the scalar nuclear spin-spin coupling constant c_4, which was calculated using density-functional theory (DFT) by Aldegunde *et al.* [46]. We estimate that the uncertainty in c_4 is ±30%, giving an uncertainty of ±27 kHz in the position of the $I = 5$ state relative to the degeneracy-weighted hyperfine centroid. The Zeeman shift is determined by the nuclear shielding constants, also from DFT [46], but we estimate that the uncertainties in these shieldings cause an uncertainty of only ±1 kHz. These uncertainties are included as a separate "theoretical" uncertainty in the final value of the ground-state binding energy.

We selectively address different hyperfine sublevels of the rovibrational ground state by changing the polarization of the Stokes laser [12] while keeping the pump laser polarization fixed parallel to the quantization axis. The weakly bound state from which we begin our STIRAP transfer has a total angular momentum projection quantum number $M_F = +4$. In the case of Stokes polarization parallel to the quantization

TABLE II. Summary of each independent measurement of the binding energy in the ground state. Both the magnetic field and the polarization of the pump light are vertical (V_P). The Stokes light may be either vertical (V_S) or horizontal (H_S) to access ground-state hyperfine levels with either $M_F = 4$ or $M_F = 5$. For each measurement we list the absolute frequency difference measured for each laser ($\nu_{\text{Stokes}} - \nu_{\text{pump}}$), the magnetic field during that measurement (B), and the binding energy of the ground state at zero field (D_0). Statistical uncertainties are shown; additional systematic uncertainties apply as explained in the text. The asterisk indicates a measurement using two-photon spectroscopy via the intermediate $|\Omega' = 0, v' = 35, J' = 1\rangle$ state. All other measurements rely on optimization of the round-trip STIRAP efficiency via the intermediate $|\Omega' = 1, v' = 29, J' = 1\rangle$ state.

Polarization	M_F	$\nu_{\text{Stokes}} - \nu_{\text{pump}}$ (MHz)	B (G)	D_0/h (MHz)
V_P, V_S	4	114 258 362.874(8)	181.542(3)	114 268 135.232(10)
V_P, H_S	5	114 258 363.067(6)	181.538(6)	114 268 135.230(14)
V_P, H_S	5	114 258 363.075(8)	181.552(4)	114 268 135.207(12)
V_P, H_S*	5	114 258 363.2(5)	181.510(3)	114 268 135.4(5)
V_P, H_S	5	114 258 363.048(5)	181.519(2)	114 268 135.253(7)

axis, we drive π transitions and address a ground state where the M_F value is unchanged. If, on the other hand, the Stokes polarization is perpendicular to the quantization axis, we drive $\sigma^{\pm}$ transitions and address ground states with either $M_F = +3$ or $M_F = +5$.

In Fig. 5, we see the effect of scanning the Stokes laser frequency on the efficiency of STIRAP transfer for both parallel and perpendicular polarizations. The coupling strengths to the hyperfine ground states are such that we have sufficient laser power to populate only two of the available hyperfine states, which are separated in energy by 0.194(10) MHz. The measured energy difference, in combination with knowledge of the states accessible with different Stokes polarizations, allows us to identify the two states with $M_F = +5$ and $M_F = +4$ as indicated in Fig. 1(c), agreeing with previous results [12]. Weak couplings to the $M_F = +3$ states mean that we have not been able to observe them. Both of these Zeeman states correlate with the $I = 5$ hyperfine state. Because of mixing between the $I = 4$ and the $I = 5$ states in a magnetic field, the measured splitting of 0.194(10) MHz has some dependence on the spin-spin coupling constant c_4. It corresponds to a value $c_4 = 0.023(7)$ MHz, which agrees within its error bars with the value of 0.1734 MHz from DFT calculations [46] and is also consistent with our attribution of an uncertainty of 30% to the latter value. We note that at a field of ~181.5 G the $M_F = +5$ state is the lowest-energy sublevel, as shown in Fig. 1(c).

We must also consider the effect of the uncertainty in the magnetic field. We have considered the atomic and molecular Zeeman shifts separately above, but with the uncertainty in the field they must be considered together. We multiply the uncertainty in the measured field by the difference in magnetic moment between the Feshbach and the ground states to give the associated uncertainty in the binding energy. This is reported in Table I and is added to the uncertainty from the frequency difference measurement above to give the total statistical uncertainty in the binding energy.

VI. MEASUREMENT CAMPAIGN

We have repeated the measurement outlined in Sec. V five times, on different days, and observed similar results for the energy difference each time, within experimental errors. In this section, we combine these measurements to give the value of the binding energy D_0. All five measurements are summarized in Fig. 7, and the precise values for each measurement are listed in Table II.

The filled red circle in Fig. 7 uses the $|\Omega' = 0, v' = 35, J' = 1\rangle$ intermediate state. The polarizations are such that we expect to address the $M_F = 3$ and 5 states, but the large spectroscopic linewidth means that this measurement does not resolve the ground-state hyperfine structure. The main purpose of this measurement is to confirm that we have identified the frequency comb tooth correctly. The other four measurements use the $|\Omega' = 1, v' = 29, J' = 1\rangle$ state in the coupled $A^1\Sigma^+ + b^3\Pi$ potential. Of these, three are measured with the $M_F = 5$ ground-state hyperfine level, and one uses the $M_F = 4$ state.

Following the procedure in the previous sections, we calculate values for binding energies for each measurement. Taking a weighted mean [47] we get a final value for the binding energy of ^{87}Rb^{133}Cs of

$$D_0 = h \times 114\,268\,135.24(4)(3)\ \text{MHz}$$
$$= hc \times 3811.574\,714\,0(13)(9)\ \text{cm}^{-1}.$$

The first uncertainty arises from the experimental error and the second one arises from the theoretical uncertainties in the ground-state hyperfine structure. Our experimental measurements of the energy difference between the initial Feshbach state and the final ground state are more accurate by one order of magnitude.

This value is a 500-fold improvement in accuracy over previous measurements averaging 3811.5759(8) cm^{-1} [13,18]. The most precise determinations of molecular binding energy we know of are precisions of $\Delta E/E \sim 10^{-8}$. These are in ^{40}K^{87}Rb, which is measured with 8×10^{-9} precision at a finite magnetic field [11], and H_2, with 1×10^{-8} precision [48]. Our fractional uncertainty is 4×10^{-10}, and improved models and measurements of the Feshbach and ground-state structure could reduce this as far as 5×10^{-11}.

VII. CONCLUSIONS

We have measured the binding energy of the ^{87}Rb^{133}Cs molecule as $h \times 114\,268\,135.24(4)(3)$ MHz using an optical frequency comb based on difference frequency generation [34,49]. The results for different intermediate states

~1.65 THz apart agree within their experimental uncertainty and we are able to resolve the nuclear Zeeman splitting of the molecular ground state. The accuracy of our ground-state binding energy measurement is limited by uncertainties in the theoretical models of the molecular structure. This is, to our knowledge, the most accurate determination to date of the dissociation energy of a molecule. The ability to measure molecular transitions with a high precision is highly relevant to proposed searches for variations in fundamental constants [8–10,19–24].

The experimental results and analysis presented in this paper are available at doi:10.15128/r244558d28c.

ACKNOWLEDGMENTS

We would like to thank the group of M. P. A. Jones for providing the Sr $^1S_0 \rightarrow {}^3P_1$ reference for the wavemeter calibrations, I. G. Hughes for useful discussions on error analysis, and B. Lu, Z. Ji, and M. P. Köppinger for their work on the early stages of the project. This work was supported by the U.K. Engineering and Physical Sciences Research Council (EPSRC) (Grants No. EP/H003363/1, No. EP/I012044/1, and No. GR/S78339/01). R.K. was supported by the EU through the Marie Curie Initial Training Network "COHERENCE" under Grant No. FP7-PEOPLE-2012-ITN-265031.

[1] L. Santos, G. V. Shlyapnikov, P. Zoller, and M. Lewenstein, Phys. Rev. Lett. **85**, 1791 (2000).
[2] M. A. Baranov, M. Dalmonte, G. Pupillo, and P. Zoller, Chem. Rev. **112**, 5012 (2012).
[3] D. DeMille, Phys. Rev. Lett. **88**, 067901 (2002).
[4] S. Ospelkaus, K.-K. Ni, D. Wang, M. H. G. de Miranda, B. Neyenhuis, G. Quéméner, P. S. Julienne, J. L. Bohn, D. S. Jin, and J. Ye, Science **327**, 853 (2010).
[5] R. V. Krems, Phys. Chem. Chem. Phys. **10**, 4079 (2008).
[6] T. A. Isaev, S. Hoekstra, and R. Berger, Phys. Rev. A **82**, 052521 (2010).
[7] J. J. Hudson, D. M. Kara, I. J. Smallman, B. E. Sauer, M. R. Tarbutt, and E. A. Hinds, Nature **473**, 493 (2011).
[8] D. DeMille, S. Sainis, J. Sage, T. Bergeman, S. Kotochigova, and E. Tiesinga, Phys. Rev. Lett. **100**, 043202 (2008).
[9] V. V. Flambaum and M. G. Kozlov, Phys. Rev. Lett. **99**, 150801 (2007).
[10] T. Zelevinsky, S. Kotochigova, and J. Ye, Phys. Rev. Lett. **100**, 043201 (2008).
[11] K.-K. Ni, S. Ospelkaus, M. H. G. de Miranda, A. Pe'er, B. Neyenhuis, J. J. Zirbel, S. Kotochigova, P. S. Julienne, D. S. Jin, and J. Ye, Science **322**, 231 (2008).
[12] T. Takekoshi, L. Reichsöllner, A. Schindewolf, J. M. Hutson, C. R. Le Sueur, O. Dulieu, F. Ferlaino, R. Grimm, and H.-C. Nägerl, Phys. Rev. Lett. **113**, 205301 (2014).
[13] P. K. Molony, P. D. Gregory, Z. Ji, B. Lu, M. P. Köppinger, C. R. Le Sueur, C. L. Blackley, J. M. Hutson, and S. L. Cornish, Phys. Rev. Lett. **113**, 255301 (2014).
[14] J. W. Park, S. A. Will, and M. W. Zwierlein, Phys. Rev. Lett. **114**, 205302 (2015).
[15] M. Guo, B. Zhu, B. Lu, X. Ye, F. Wang, R. Vexiau, N. Bouloufa-Maafa, G. Quéméner, O. Dulieu, and D. Wang, Phys. Rev. Lett. **116**, 205303 (2016).
[16] U. Gaubatz, P. Rudecki, S. Schiemann, and K. Bergmann, J. Chem. Phys. **92**, 5363 (1990).
[17] K. Bergmann, H. Theuer, and B. W. Shore, Rev. Mod. Phys. **70**, 1003 (1998).
[18] M. Debatin, T. Takekoshi, R. Rameshan, L. Reichsöllner, F. Ferlaino, R. Grimm, R. Vexiau, N. Bouloufa, O. Dulieu, and H.-C. Nägerl, Phys. Chem. Chem. Phys. **13**, 18926 (2011).
[19] E. Reinhold, R. Buning, U. Hollenstein, A. Ivanchik, P. Petitjean, and W. Ubachs, Phys. Rev. Lett. **96**, 151101 (2006).
[20] E. R. Hudson, H. J. Lewandowski, B. C. Sawyer, and J. Ye, Phys. Rev. Lett. **96**, 143004 (2006).
[21] S. Truppe, R. J. Hendricks, S. K. Tokunaga, H. J. Lewandowski, M. G. Kozlov, C. Henkel, E. A. Hinds, and M. R. Tarbutt, Nat. Commun. **4**, 2600 (2013).
[22] B. H. McGuyer, M. McDonald, G. Z. Iwata, M. G. Tarallo, A. T. Grier, F. Apfelbeck, and T. Zelevinsky, New J. Phys. **17**, 055004 (2015).
[23] B. H. McGuyer, M. McDonald, G. Z. Iwata, M. G. Tarallo, W. Skomorowski, R. Moszynski, and T. Zelevinsky, Nat. Phys. **11**, 32 (2015).
[24] S. Taie, S. Watanabe, T. Ichinose, and Y. Takahashi, Phys. Rev. Lett. **116**, 043202 (2016).
[25] M. L. Harris, P. Tierney, and S. L. Cornish, J. Phys. B **41**, 035303 (2008).
[26] D. L. Jenkin, D. J. McCarron, M. Köppinger, H. W. Cho, S. A. Hopkins, and S. L. Cornish, Eur. Phys. J. D **65**, 11 (2011).
[27] H. W. Cho, D. J. McCarron, D. L. Jenkin, M. P. Köppinger, and S. L. Cornish, Eur. Phys. J. D **65**, 125 (2011).
[28] D. J. McCarron, H. W. Cho, D. L. Jenkin, M. P. Köppinger, and S. L. Cornish, Phys. Rev. A **84**, 011603 (2011).
[29] M. P. Köppinger, D. J. McCarron, D. L. Jenkin, P. K. Molony, H.-W. Cho, S. L. Cornish, C. R. Le Sueur, C. L. Blackley, and J. M. Hutson, Phys. Rev. A **89**, 033604 (2014).
[30] T. Takekoshi, M. Debatin, R. Rameshan, F. Ferlaino, R. Grimm, H.-C. Nägerl, C. R. Le Sueur, J. M. Hutson, P. S. Julienne, S. Kotochigova, and E. Tiemann, Phys. Rev. A **85**, 032506 (2012).
[31] P. D. Gregory, P. K. Molony, M. P. Köppinger, A. Kumar, Z. Ji, B. Lu, A. L. Marchant, and S. L. Cornish, New J. Phys. **17**, 055006 (2015).
[32] L. P. Yatsenko, V. I. Romanenko, B. W. Shore, and K. Bergmann, Phys. Rev. A **65**, 043409 (2002).
[33] P. K. Molony, P. D. Gregory, A. Kumar, C. R. Le Sueur, J. M. Hutson, and S. L. Cornish, ChemPhysChem (2016), doi:10.1002/cphc.201600501.
[34] H. Telle, Method for generating an offset-free optical frequency comb and laser apparatus therefor, European Patent Application EP1594020 (2005).
[35] T. Fuji, A. Apolonski, and F. Krausz, Opt. Lett. **29**, 632 (2004).
[36] E. Benkler, H. R. Telle, A. Zach, and F. Tauser, Opt. Express **13**, 5662 (2005).
[37] T. Puppe, A. Sell, R. Kliese, N. Hoghooghi, A. Zach, and W. Kaenders, Opt. Lett. **41**, 1877 (2016).
[38] Jackson Labs Fury GPS reference.

[39] Agilent N9320B spectrum analyzer for the Stokes laser; Agilent N1996 spectrum analyzer for the pump laser.
[40] High Finesse WS-U wavemeter.
[41] ISOMET 532B fixed-frequency driver/amplifiers.
[42] Agilent N1996 spectrum analyzer referenced to the 10-MHz GPS clock.
[43] E. D. Black, Am. J. Phys. **69**, 79 (2001).
[44] S. Bize, Y. Sortais, M. S. Santos, C. Mandache, A. Clairon, and C. Salomon, Europhys. Lett. **45**, 558 (1999).
[45] Daniel A. Steck, Alkali D Line Data, available online at http://steck.us/alkalidata.
[46] J. Aldegunde, B. A. Rivington, P. S. Zuchowski, and J. M. Hutson, Phys. Rev. A **78**, 033434 (2008).
[47] I. G. Hughes and T. P. A. Hase, *Measurements and Their Uncertainties: A Practical Guide to Modern Error Analysis* (Oxford University Press, Oxford, UK, 2010).
[48] J. Liu, E. J. Salumbides, U. Hollenstein, J. C. J. Koelemeij, K. S. E. Eikema, W. Ubachs, and F. Merkt, J. Chem. Phys. **130**, 174306 (2009).
[49] D. Fehrenbacher, P. Sulzer, A. Liehl, T. Kälberer, C. Riek, D. V. Seletskiy, and A. Leitenstorfer, Optica **2**, 917 (2015).